Fabrication of composite poly(D,L-lactide)/montmorillonite nanoparticles for controlled delivery of acetaminophen by solvent-displacement method using glass capillary microfluidics

Rahimah Othman[a,b*], Goran T. Vladisavljević[a*], Noreen L. Thomas[c], Zoltan K. Nagy[a,d]

[a]*Department of Chemical Engineering, Loughborough University, Ashby Road, Loughborough, Leicestershire LE11 3TU, UK*

[b]*School of Bioprocess Engineering, Universiti Malaysia Perlis, Kompleks Pusat Pengajian Jejawi 3, 02600 Arau, Perlis, Malaysia*

[c]*Department of Materials, Loughborough University, Ashby Road, Loughborough, Leicestershire LE11 3TU, UK*

[d]*School of Chemical Engineering, Purdue University, West Lafayette, IN 47907-2100, USA*

** Corresponding author: Email R.Othman@lboro.ac.uk, G.Vladisavljevic@lboro.ac.uk*

Manuscript statistics: 5995 words, 5 figures and 3 tables

ABSTRACT

Paracetamol (PCM)-loaded composite nanoparticles (NPs) composed of a biodegradable poly(D,L-lactide) (PLA) polymer matrix filled with organically modified montmorillonite (MMT) nanoparticles were fabricated by antisolvent nanoprecipitation in a microfluidic co-flow glass capillary device. The incorporation of MMT in the polymer improved both the drug encapsulation efficiency and the drug loading, and extended the rate of drug release in simulated intestinal fluid (pH 7.4). The particle size increased on increasing both the drug loading and the

concentration of MMT in the polymer matrix, and decreased on increasing the aqueous to organic flow rate ratio. The drug encapsulation efficiency in the NPs was higher at higher aqueous to organic flow rate ratio due to faster formation of the NPs. The PCM-loaded PLA NPs containing 2 wt% MMT in PLA prepared at an aqueous to organic flow rate ratio of 10 with an orifice size of 200 μm exhibited a spherical shape with a mean size of 296 nm, a drug encapsulation efficiency of 38.5% and a drug loading of 5.4%. The encapsulation of MMT and PCM in the NPs was confirmed by transmission electron microscopy, energy dispersive x-ray spectroscopy, x-ray diffraction, differential scanning calorimetry, thermogravimetric analysis and attenuated total reflection-Fourier transform infrared spectroscopy.

Keywords: Montmorillonite; Acetaminophen; Biodegradable Nanoparticles; Controlled Drug Release; Microfludics; Nanoprecipitation

1. Introduction

Many drugs are insoluble in aqueous media and biological fluids and, thus, their effects are diminished due to poor bioavailability. To enhance their solubility, drug molecules can be incorporated in the interlayer space of layered clays [1]. Montmorillonite (MMT) is a natural clay mineral that belongs to the smectite group, in which a central alumina octahedral sheet is sandwiched between two silica tetrahedral sheets with a thickness of individual layers of ≤1 nm. The imperfection of the crystal lattice and the isomorphous substitution of Mg^{2+} for Al^{3+} induces a net negative charge that leads to the adsorption of alkali and alkaline-earth metal cations in the interlayer space [2]. These cations can be exchanged with cationic forms of therapeutic molecules and drugs. The examples of such active species adsorbed onto MMT by cationic

bonding are protonated forms of amino acids [3], promethazine chloride [4], timolol maleate [5], buformin hydrochloride [6], 5-fluorouracil [7], sertraline [8], vitamin B1 [2, 5] and buspiron hydrochloride [9]. Anionic drugs can be intercalated into the interlayer space of MMT by hydrogen bonding between their functional groups and hydroxyl groups or oxygen atoms in MMT. For example, ibuprofen was adsorbed due to hydrogen bonding between its $-COO^-$ groups and hydroxyl groups of MMT [10].

MMT exhibits high drug loading capacity due to high specific surface area, and provides mucoadhesive properties required for drug delivery across the gastrointestinal barrier [11-13]. MMT has been proved to be nontoxic by hematological, biochemical and histopathological analyses [14]. MMT is a highly efficient detoxifier which has been used in the treatment of open wounds, hemorrhoids, stomach ulcers, intestinal problems and other diseases [7, 15, 16].

Paclitaxel- and docetaxel-loaded PLGA/MMT nanoparticles (NPs) have been prepared by an emulsion/solvent evaporation method using dichloromethane as organic solvent for PLGA [12, 17]. MMT was added to the aqueous phase and adsorbed onto the surface of the polymer NPs after solvent evaporation. Due to its hydrophilic nature, MMT is incompatible with most polymers and must be chemically modified to be incorporated within the polymer matrix. MMT can be rendered hydrophobic by replacing inorganic cations in the interlayer space with organic alkylammonium or alkylphosphonium cations [13, 18-19]. Lee *et al.* [20] encapsulated paracetamol within Eudragit® S100 microspheres using water-in-oil-in-oil double emulsion-solvent evaporation method. Shimokawa *et al.* [21] prepared gelatin microcapsules loaded with the pain-relieving drug phenacetin by a simple coacervation technique. Lai and Tsiang [22] produced PLA microcapsules containing paracetamol using O/W and W/O/W emulsion-solvent evaporation methods.

In this work, nanoprecipitation induced by microfluidic micromixing was used to produce novel composite paracetamol-loaded NPs consisting of organically modified MMT incorporated into poly(D,L-lactide) (PLA) NPs (hereinafter called the PLA/MMT NPs). PLA is a biodegradable and bioresorbable polymer [1] widely used as a drug carrier. The inclusion of organically modified MMT into the polymer matrix has proven to be a viable strategy to improve the thermal, mechanical, and barrier properties of PLA sheets [18, 23]. In this work, MMT was incorporated into PLA NPs to increase drug bioavailablity and modify its release. Paracetamol (acetaminophen, $C_8H_9NO_2$) was chosen as a model drug due to its significant therapeutic effects against a wide variety of arthritic and rheumatic conditions involving musculoskeletal pain and other painful disorders [24-26].

Nanoprecipitation (solvent displacement) is a low-energy process for preparation of NPs driven by spontaneous counter-diffusion of polymer-laden amphiphilic organic solvent and water [27-29]. Nanoprecipitation gives smaller polymeric NPs than emulsion-solvent evaporation and allows the use of non-halogenated organic solvents which are less toxic than halogenated solvents typically used in emulsion-solvent evaporation.

A crucial challenge in nanoprecipitation is to control the mixing conditions in order to produce uniformly sized particles [30]. The capability of microfluidic devices to rapidly mix fluids, continuously vary reaction conditions, and provide homogeneous reaction environments and small reactor volumes has made them attractive tools for a myriad of applications [31-32]. Flow focusing polydimethylsiloxane (PDMS) devices are widely used for production of NPs [30]. However, PDMS swells in contact with organic solvents and the fabrication of PDMS devices by soft lithography requires the use of a master mould that must be manufactured using expensive photolithographic techniques. In this work, axisymmetric glass capillary devices were

used [33] that are cheap to fabricate and have superior solvent resistance and optical properties for *in-situ* visual control of the process. These devices have been used by our group to prepare liposomes loaded with vitamin E [34], polymeric micelles [35] and polycaprolactone NPs [36-37].

The aim of this study was: (i) to investigate the possibility of efficiently incorporating MMT and paracetamol into PLA NPs by microfluidic mixing/nanoprecipitation; (ii) to study the effect of MMT on the physical properties of the prepared NPs; and (iii) to investigate the encapsulation efficiency of paracetamol inside the NPs and their *in vitro* drug release behaviour.

2. Materials and Methods

2.1. Materials

Poly(D,L-lactide) (PLA, Ingeo^{TM} 4060D) was supplied by Natureworks LLC (Minetonka, MN, USA). 4060D is an amorphous polymer with a content of D- and L -lactide of 12 and 88 mol%, respectively, a density of 1,240 kg m^{-3}, a glass transition temperature of 55-60^{o}C, and a weight-average molecular weight (M_w) of 89,000 g mol^{-1}, as determined by gel permeation chromatography. Tetrahydrofuran (THF), HPLC grade (purity≥99.9%) was purchased from Sigma-Aldrich, UK. Polyvinyl pyrrolidone (PVP, M_w = 360,000 g mol^{-1}) obtained from Sigma-Aldrich was used as a stabiliser to prevent agglomeration and coalescence of the NPs. Paracetamol (PCM) (purity ≥ 99.9%) was purchased from Fisher Scientific, UK.

MMT used in this work was Cloisite® 30B with a density of 1,980 kg m^{-3} obtained from Southern Clay Products (Gonzales, TX, USA). It is MMT organically modified with N,N-Bis(2-hydroxyethyl)-N-methyl-N-tallow ammonium chloride to improve its compatibility with the polymer matrix. PLA/MMT nanocomposite films were prepared by melt intercalation [18].

Briefly, PLA granules were dried at 60°C in a vacuum oven and then melt blended with 20 wt% of organo-MMT at 170°C to make a masterbatch. The masterbatch was then mixed with dried PLA granules at 170°C to form nanocomposites containing 2, 5, and 20 wt% of the clay. The organic phase was prepared by dissolving PCM and pure PLA or PLA/MMT composite film in THF and contained 6 g L^{-1} of the excipient (PLA or PLA/MMT) and 1.2-4.2 g L^{-1} of PCM. The aqueous phase was 0.2 wt% PVP dissolved in Milli-Q water.

2.2. Preparation of PCM loaded PLA and PLA/MMT NPs

The NPs were prepared using a co-flow glass capillary device consisting of a round capillary with a tapered tip inserted into a square capillary (Fig. 1a). Two 11 Elite syringe pumps (Harvard Apparatus, UK) were used to deliver the organic and aqueous phase from SGE syringes to the device. The organic phase was injected through the inner capillary (1 mm O.D. and 0.58 mm I.D.) with an orifice diameter of 200 μm via a Teflon tubing, which is highly resistant to THF. The aqueous phase was delivered co-currently through the outer square capillary (1.05 mm inner dimension). PLA precipitated almost instantaneously in the square capillary when the two fluids were brought into contact. This was recorded at 25 frames/second and 576 × 288 resolution using a Phantom V9.0 high-speed camera (Vision Research, Ametek, US) attached to an inverted microscope. The aqueous phase flow rate (Q_{aq}) was 5 mL h^{-1} and the organic phase flow rate (Q_{or}) ranged from 0.5 to 3.3 mL h^{-1} to give Q_{aq}/Q_{or} between 10 and 1.5. The duration of each experiment was 30 min.

A micrograph of the mixing zone within the glass capillary device at Q_{aq}/Q_{or} = 1.5 captured by the high-speed camera is shown in Fig. 1a. The interface between the aqueous and organic phases is visible, although THF and water are miscible in all proportions and have zero equilibrium interfacial tension. When two miscible liquids are suddenly put into contact,

concentration gradients at the boundary give rise to a transient tension between the liquids, σ given by [38]: $\sigma = k\Delta C^2 / \delta$, where k is the proportionality constant, ΔC is the change in concentration over the interfacial layer and δ is the thickness of the boundary layer. The interface was found to be blurred on the front side of the jetbecause of better mixing near the axis of the collection capillary due to high fluid velocities. The distortion of the interface known as "viscous fingering" is also noticeable. When a less viscous fluid is injected at high velocity into a more viscous one, a part of the more viscous fluid forms finger-like patterns due to non-uniform penetration. At 293 K, the viscosities of THF and water are 0.63 and 1 mPa·s respectively, supporting this assumption. Due to the 3D geometry of the micromixer, the continuous phase fully surrounds the organic phase and de-wets it from the walls (Fig. 1a). Since the liquid/liquid interface is fully displaced from the walls and the NPs are formed at this interface, the deposition of the NPs onto the reactor walls is minimised. In a planar geometry, the organic phase wets the channel walls at the inlet, which can compromise the resultant particle size due to particle deposition onto the walls. A possible structure of encapsulated PCM-PLA/MMT NPs is depicted in Fig.1b with Na^+ ions replaced by quaternary ammonium cations on the surface of the platelets. Paracetamol molecules and PLA chains are present between individual MMT platelets.

2.3. Determination of drug content

The organic solvent was completely evaporated from the prepared nanosuspension using a vacuum oven (Technico, Fistreem International Ltd, Loughborough, UK) at room temperature under a pressure of less than 10 Torr. The nanosuspension was then ultracentrifuged (Heraeus Labofuge 400R centrifuge, Thermo Scientific) at 15,000 rpm (23,000*g*) for 1 h. The supernatant containing the dissolved free drug was separated from the sediment, diluted with milli-Q water

by a factor of 16 and analysed. The concentration of PCM in the supernatant was determined using a Shimadzu model UV-2550 UV-visible spectrophotometer at a wavelength of 243 nm [39]. The drug encapsulation efficiency was calculated as:

$$\%E.E. = [1-(M_R / M_T)] \times 100\% \quad (1)$$

where M_R is the mass of drug in the supernatant and M_T is the total mass of drug in the sample [39-41]. The drug loading of the NPs was determined as:

$$\%D.L. = [(M_T - M_R) / M_{NP})] \times 100\% \quad (2)$$

where M_{NP} is the total mass of NPs in the sample [36].

2.4. Characterisation of the prepared NPs

2.4.1. Particle size measurement

The size distribution of the NPs was determined by dynamic light scattering using a Delsa^{TM} Nano HC Particle Analyzer (Beckman Coulter, Inc), which measures the fluctuation in the intensity of scattered light as a function of time. Smaller particles cause the intensity to fluctuate more rapidly than large particles. The nanosuspension was diluted 5-fold by Mili-Q water before being transferred into a 4 mL disposable cuvette and placed into the instrument. The measurement time was 120 s. The measurements were repeated three times at a scattering angle of 165° and a temperature of 25°C using CONTIN and Cumulants methods. The Cumulants method provides a *Z*-average value and a polydisperity index, PDI (a dimensionless measure of the breadth of the size distribution) [42].

2.4.2. Transmission electron microscopy (TEM) and energy-dispersive X-ray spectroscopy (EDS)

The internal structure of the NPs was investigated using TEM. A drop of the sample was deposited onto a carbon-coated copper mesh and left to dry before observation in a JEOL JEM-2000FX transmission electron microscope operated at an accelerating voltage of 200 kV. Elemental analysis of the samples was performed by EDS using an Oxford Instruments Inca EDX system.

2.4.3. Differential scanning calorimetry (DSC)

Modulated Differential Scanning Calorimetry (DSC) was performed using a TA Instruments Model 2910 calorimeter. 5-10 mg of the sample (pure PLA, pure PCM, physical mixture of PLA and PCM, PCM-loaded PLA NPs and PCM-loaded PLA/MMT NPs) was used. PCM-loaded NPs were prepared by freeze-drying the sediment after centrifugation in a freeze dryer (Edwards, type EF4 Modulyo). The sample was placed in an aluminium pan and hermetically sealed. The sample pan was heated from 30 to 220 °C using a scanning rate of 10 °C min^{-1} and compared with an empty pan. Dry nitrogen at 60 mL min^{-1} was used as the purge gas. Triple runs were carried out on each sample to check reproducibility.

2.4.4. Thermogravimetric analysis (TGA)

The thermal stability of the NPs was assessed by TGA (Q5000IR Thermogravimetric Analyzer) at a heating rate of $10^{o}C$ min^{-1} over the temperature range of 20-$600^{o}C$ under dry nitrogen as the effluent gas.

2.4.5. X-ray diffractometry (XRD)

Wide angle X-ray diffraction was performed using a Bruker D8 diffractometer by exposing samples to CuKa radiation (40 kV, 20 mA) over the 2θ range from 10^o to 40^o, with a step size of 0.02^o, an acquisition time per step of 5 s and a scanning speed of 0.5° min^{-1}. The samples were prepared by injection moulding under nitrogen at 100°C and transferred at ambient temperature to a circular mold with a diameter of 20 mm and a thickness of 1 mm.

2.4.6. Attenuated total reflection-Fourier transform infrared (ATR-FTIR) spectroscopy

ATR-FTIR spectra in the range of 4000-400 cm^{-1} were recorded on a Thermo Scientific Nicolet iS50 ATR spectrometer with a monolithic diamond crystal. 2-3 mg of the powdered sample was placed onto the Universal diamond ATR top-plate and the spectrum was acquired within 32 s.

2.4.7. In vitro drug release measurements

In-vitro drug release tests were carried out using PCM-loaded PLA and PLA/2 wt% MMT NPs in two different release media: Mili-Q water (the control fluid) and 0.01 M sodium phosphate-buffered saline (PBS) at pH 7.4 (the simulated intestinal fluid). Simulated intestinal fluid (pH=7.4) was chosen since paracetamol is a weak acid and should have a higher solubility in intestinal fluid than in simulated gastric fluid (pH=1.2). An aliquot of the prepared suspension was vacuum-evaporated in order to remove THF. The suspension was then transferred in a test tube and incubated in a shaking bath at 50 rpm and 37 °C to mimic the human blood stream conditions [40]. At predetermined time intervals, the test tube was taken out of the shaker and centrifuged at 15,000 rpm for 1 h at room temperature. The supernatant was removed and used to

measure the amount of drug released. The dissolution medium was replenished with fresh Mili-Q water or PBS to keep the total volume of the release medium constant.

3. Results and discussion

3.1. Control over the average size of the prepared NPs

Table 1 shows the effect of drug-to-excipient ratio in the organic phase and the type of excipient on the average particle size, drug encapsulation efficiency and drug loading of the prepared NPs at the flow rate ratio of 10. The average particle size increased from 285 to 398 nm for PLA and from 296 to 428 nm for PLA/2 wt% MMT with an increase in the drug-to-excipient ratio in the organic phase from 0.2 to 0.7. The average size of composite NPs was bigger than that of the pure PLA NPs, due to the incorporation of MMT into the polymer matrix. A similar effect has been reported for docetaxel-loaded NPs when MMT was incorporated into the polymer matrix [17].

The drug loading in PLA NPs increased from 5.9 to 10.9 % as the drug-to-excipient ratio in the organic phase increased from 0.2 to 0.7 (Table 1). However, the drug encapsulation efficiency decreased from 35 to 27 % on increasing the drug loading in the NPs. Low drug encapsulation efficiencies can be attributed to the high solubility of PCM in water of 12.8 mg mL^{-1} at 20 °C [43]. Since the concentration of PCM in the organic phase was 1.2-4.2 g L^{-1} and Q_{aq}/Q_{or} was 10, the concentration of PCM in the suspension after THF evaporation was 0.12-0.42 mg mL^{-1}, which is only 1-3% of the saturation point of PCM in water. Therefore, without entrapment within the NPs, all PCM added to the organic phase would dissolve completely in the aqueous phase. The specific surface area of the prepared NPs is another factor contributing to the significant loss of PCM into the aqueous phase. A decrease in drug entrapment with increased drug loading was probably due to the more porous polymer matrix formed as a result of the

dissolution of PCM from the surface regions of the NPs. Owing to the increased amount of drug loaded, a more porous matrix may be formed through which the drug can easily escape to the aqueous phase, thereby decreasing the content of PCM encapsulated [44]. Niwa et al. [45] also observed decreased drug entrapment at high drug loadings due to enhanced drug leakage into the aqueous phase.

Table 2 shows the effect of Q_{aq}/Q_{or} and the type of carrier on the particle size and drug loading. Some initial research has been done to determine the particle size in THF of organo-modified non-intercalated MMT and dissolved PLA/MMT composite films. The size of intercalated/exfoliated MMT particles prepared by dissolving PLA/MMT films in THF at 1 g L^{-1} was (41 ± 6.1), (39 ± 4.0), and (78 ± 8.4) nm for the composite films containing respectively 2, 5, and 20 wt% of MMT. The particle size of pure MMT in THF was (426 ± 21.2) nm at 0.25 g L^{-1}. After intercalation/exfoliation, MMT platelets are partially or fully separated from each other and therefore, the size of polymer-intercalated MMT particles is smaller than the size of non-intercalated/agglomerated particles. This observation proves that PLA was successfully intercalated into MMT and that PLA/MMT composite films were more suitable as drug carriers than a mechanical mixture of MMT and PLA powders. In all cases, the size of MMT NPs in the organic phase was significantly lower than the orifice diameter (200 μm).

The size of PLA/MMT NPs increased on increasing the content of MMT in the polymer matrix from 2 to 20 wt% and was larger than the size of pure PLA NPs (Table 2). The size of NPs decreased as the flow rate ratio increased, which was more pronounced for composite NPs. A higher flow rate ratio provides more rapid mixing due to higher flow rate in the collection capillary [41, 42]. When fluids are mixed more rapidly, the critical degree of supersaturation needed for nucleation is reached faster, which leads to the generation of more nuclei per unit

time. Since the growth of nuclei is limited by the amount of available polymer in the liquid phase, it results in smaller NPs. In addition, at higher Q_{aq}/Q_{or} values, the NPs are more diluted after formation, which suppresses the rate of particle growth and agglomeration, due to the lower frequency at which the NPs collide with each other. Smaller NPs at higher Q_{aq}/Q_{or} values have also been reported in membrane contactors [35, 46, 47] and flow focusing microfluidic devices [48].

Table 2 also includes the drug encapsulation efficiency and drug loading at a PCM concentration in the organic phase of 20 wt% for various Q_{aq}/Q_{or} values and two different drug-carriers, pure PLA and PLA/2 wt% MMT. The drug encapsulation efficiency and drug loading in the NPs increased with increasing Q_{aq}/Q_{or}, probably due to faster nucleation and faster inclusion of drug molecules within the polymer matrix. The incorporation of MMT into the polymer matrix improved both the drug entrapment efficiency and drug loading. This was due to reduced porosity of the composite polymer matrix compared with that of the pure polymer [49, 50], adsorption of PCM onto the nanoclay particles and an increased diffusion path length of PCM molecules within the polymer.

3.2. Characterisation of the NPs

3.2.1. TEM and elemental analysis of the NPs

Fig. 2 shows the transmission electron micrographs of the NPs containing different concentrations of MMT in the polymer matrix. Only PLA and PLA/ 2wt% MMT NPs were found to have a spherical shape with a smooth surface. Clay platelets are visible in all NPs containing 2 wt% MMT, but the clay is incorporated entirely in the interior of the NP.

Due to the 2D structure of MMT platelets and their very low thickness compared with the diameter of a composite nanoparticle (individual platelet thicknesses are just 1 nm and the particle diameter was at least 300 nm), although 80% of the particle cross section was occupied by the MMT platelets, it was found that the volume of MMT was very low compared with the total particle volume. As a result of higher loading of MMT in the polymer matrix, the shape of NPs containing 5 and 20 wt% of MMT in the polymer matrix is distorted and significantly deviates from a spherical shape. The last two figures in Fig. 2 show TEM images of drug-loaded NPs prepared with the drug-to-excipient mass ratio in the organic phase of 1:5. Drug-loaded PLA NPs are spherical and exhibit a smooth surface and homogeneous interior indicating that the drug nanocrystals are finely and uniformly dispersed within the polymer matrix. Drug-loaded NPs containing 2 wt% MMT in the matrix are not perfectly spherical, due to inclusion of both MMT platelets and PCM nanocrystals in the polymer matrix. The polydispersity index of the NPs in all samples was less than 0.25.

The TEM images in Fig. 2 indicate that the nanoclay was successfully incorporated in the host polymer. Additional evidence came from the elemental analysis of the NPs (Table 3). The octahedral sheet of MMT has Al as the central atom (partly substituted by Mg and Fe) and the tetrahedral sheets have Si as the central atom. That is why Al, Mg, Fe and Si were all detected in MMT/PLA NPs but not in PLA NPs. A disproportionately high content of carbon and copper in all samples was due to carbon-coated copper grids used to hold the samples for EDS analysis. The significantly higher amount of carbon in drug-loaded NPs compared with blank PLA and PLA/MMT NPs was due to the higher mass fraction of C in paracetamol ($C_8H_9NO_2$) compared with that in PLA, $(C_3H_4O_2)_n$.

3.2.2. XRD analysis

The crystallinity of the fabricated NPs was investigated by XRD, as shown in Fig. 3a. The crystalline drug (PCM) shows sharp peaks at 13.6^o, 16.4^o, 23.2^o, 23.8^o, 26.2^o, 26.9^o and 30.8^o, which are in good agreement with the reported values [51]. The degree of crystallinity of PCM was very high (90.2%), but less than 100% because inevitably some amorphous content is generated during the processes of milling, wet granulation, drying, re-crystallization and compaction. The diffraction pattern of pure PLA powder includes only a broad 'hump' at 14.8^o, due to the amorphous nature of poly(D,L-lactide). MMT shows a characteristic diffraction peak at 2θ of 6.4° corresponding to the 001 plane with a 'd' spacing of 1.36 nm [13]. This peak cannot be seen because the 2θ axis starts at 10^o, but two minor peaks at 19.5^o and 36^o are visible and they agree with previous results [49]. The diffraction pattern of the PLA/MMT composite film shows a wide 'hump' between 2θ values of 10° and 25° and the degree of crystallinity of 69.6% is lower than that of pure MMT (76.4%). As a result of intercalation of PLA in the interlayer spacing, there is an increase in 'd' spacing. The physical mixture of PCM and PLA exhibits two characteristic sharp peaks of PCM at 13.6^o and 23.2^o, but also a broad hump due to the contribution from PLA. However, PCM peaks disappear in the diffraction pattern of PCM-loaded PLA NPs, indicating that PCM was completely incorporated inside the polymer matrix. On the other hand, PCM-loaded PLA/MMT NPs produce a series of small peaks, which reveal the presence of crystalline MMT platelets protruding from the surface of the NPs.

3.2.3. DSC analysis

Fig. 3b shows the thermograms of the prepared NPs, raw materials and physical mixtures of the drug and the polymer. The samples were heated above the melting points (T_m) of PCM. Pure PCM powder exhibited a large endothermic peak of melting with a maximum at 170^{o}C and

a shallow, broad endothermic peak at 60^{o}C corresponding to the glass transition temperature (T_g) of poly(D,L-lactide). No peak was observed in the thermogram of pure MMT due to its high thermal stability. Two endothermic peaks corresponding to the T_m of PCM and the T_g of PLA were detected in the physical mixtures of PLA and PCM, and PLA/MMT and PCM, respectively. The peaks of PCM-loaded PLA and PLA/MMT NPs were shifted to lower temperatures (~160^{o}C) indicating that PCM entrapped in the NPs was in an amorphous or disordered-crystalline phase. Moreover, the appearance of a single peak for the loaded NPs indicates that PCM was uniformly distributed in the NPs.

3.2.4. TGA

TGA was performed to determine the thermal stability of the prepared NPs. The TGA curve of MMT (Fig. 4a) shows two inflection points, at ~270^{o}C due to free water evaporation and at 370^{o}C due to the release of structural (hydroxyl) water [2, 5] with 22% weight loss recorded at 600^{o}C. For pure PLA powder, 10% degradation occurred at 319^{o}C, which signifies the onset of degradation. The midpoint was at 346^{o}C and the powder was totally decomposed to CO_2 and H_2O at 370^{o}C. PLA/MMT composite film with 2 wt% MMT was more thermally stable than pure PLA powder and the amount of non-volatile residue at 600^{o}C was 3%. The TGA curve for PCM showed a steep decrease between 230 and 300^{o}C with 99% mass loss recorded at 600^{o}C. PLA NPs were less thermally stable than pure PLA powder due to their lower degree of crystallinity, as a result of fast polymer precipitation. It has been found that fast removal of polymer-dissolving organic solvent inhibits crystallisation of the polymer, because the polymer chains have less time to pack together in an organized manner [52]. The PCM-loaded PLA NPs started to degrade at lower temperature than the blank PLA NPs due to the presence of PCM in

the polymer matrix, which is another indicator of PCM encapsulation. PCM-loaded PLA/MMT NPs were fully degraded only at 370^{o}C and were more stable than the blank PLA and PCM-loaded PLA NPs, whose complete degradation occurred at 260 and 270^{o}C, respectively. The amount of non-volatile residue in PCM-loaded PLA/MMT NPs was 2 wt%, which corresponds to the amount of MMT in the composite film, indicating that MMT was efficiently entrapped in the NPs.

3.2.5. ATR-FTIR spectroscopy

The FTIR spectra of the prepared NPs and raw materials are shown in Fig. 4b. The IR peak of pure PLA at 1760 cm^{-1} was due to the stretching vibration of the C=O bonds along the PLA chain and this peak had the same position in all samples containing PLA. The FTIR spectrum of MMT showed an absorption band at 3600 cm^{-1} due to the stretching vibration of the O-H bond in Al−OH and Si−OH. The two bands that appear at 2930 and 2850 cm^{-1} can be attributed to the asymmetric and symmetric stretching of the methylene groups (-CH_2-) in the quaternary ammonium compound used to modify MMT. The band at 1465 cm^{-1} corresponds to the bending vibration of the methylene groups of the quaternary ammonium compound. The most intense band in the FTIR spectrum of MMT occurred near 1000 cm^{-1} can be attributed to the stretching vibrations of the Si-O groups in tetrahedral sheets. The bands at 915, 875 and 836 cm^{-1} were attributed to Al-Al-OH, Al-Fe-OH and Al-Mg-OH bending vibrations, respectively [53] and the band near 500 cm^{-1} may result from the stretching of the Al-O bonds.

No peak shifts or new peaks appeared in the spectra of the blank PLA NPs compared with PLA powder, which means that FTIR could not reveal any change in the molecular structure of PLA as a result of dissolution and nanoprecipitation, as opposed to XRD and TGA analysis. New peaks between 670 and 400 cm^{-1} detected in the spectra of PLA/MMT composite film and PCM-

loaded PLA/MMT NPs, as compared with the spectrum of PLA powder, were caused by Al-O and Si-O bonds in MMT and verify the inclusion of MMT in PLA. The characteristic absorption peaks due to carbon-carbon stretching vibrations in the aromatic ring of PCM were visible in the region between 1265 and 1660 cm^{-1} for all PCM-loaded NPs. This indicates that PCM was encapsulated within the NPs, but has not strongly interacted with PLA and MMT since no peak shifts occurred [10].

3.3. In vitro release of PCM from nanoparticles

The amount of PCM released from plain PLA and hybrid PLA/MMT NPs was measured over 190 h by recording the absorbance at 243 nm (Fig. 5). Zero-time corresponds to the start of the incubation period, but the amount of PCM plotted in Fig. 5 excludes the amount of drug released during the nanoprecipitation process. For the conditions in Figure 5, the total amount of drug released during the processes of fabrication and storage ranged between 84 and 90%. A fast drug release was observed over the first 9 h which can be attributed to relatively high solubility of PCM in water. It was followed by a very slow release over a long period of time due to diffusion of the drug from the PLA cores into the dissolution media. The rate of drug release from nanoclay-loaded NPs was reduced compared to plain PLA NPs due to the more compact polymer matrix [50], a physical adsorption of PCM onto MMT and a tortuous path of drug molecules due to obstacles imposed by non-permeable clay particles randomly distributed in the polymer matrix (Fig. 1b). Slightly faster PCM release rates were found for Milli-Q water, probably due to higher solubility of PCM in pure water compared with PBS and different swelling properties of NPs in different solutions.

4. Conclusions

In this study, antisolvent nanoprecipitation in a co-flow 3D glass capillary device was used to produce paracetamol-loaded PLA/MMT NPs composed of a biodegradable polymer matrix filled with organically modified MMT clay. The size of the intercalated/exfoliated MMT particles in the organic phase was 41-78 nm. The incorporation of nanoclay in the polymer matrix improved both the drug encapsulation efficiency and drug loading in the final formulation, and extended the rate of drug release into simulated intestinal fluid. The particle size increased on increasing the drug loading and the content of MMT in the polymer matrix, and decreased with increasing aqueous to organic flow rate ratio in the glass capillary device. In addition, the drug encapsulation efficiency and drug loading in the NPs increased with increasing aqueous to organic flow rate ratio, due to more rapid mixing and faster formation of the NPs.

The 2 wt% PLA/MMT composite film was found to be the most suitable drug carrier due to the spherical shape of the fabricated NPs and almost complete inclusion of the nanoclay platelets inside the host polymer. The composite nanoclay-loaded NPs were significantly more thermally stable than the plain PLA NPs. The incorporation of MMT and PCM into PLA was confirmed by the new peaks detected in the FTIR spectra of the drug-loaded composite NPs in the regions between 670 and 400 cm^{-1} (MMT), and 1265 and 1660 cm^{-1} (PCM). In future work, the production rate of the NPs will be improved using microengineered membranes with regular pore spacing that will be used instead of glass capillaries.

Acknowledgements

The authors acknowledge the financial support given for this work through the Ministry of Higher Education Malaysia and the technical assistance by Dr Zhaoxia Zhou from the

Department of Materials at Loughborough University for TEM analysis. We kindly thank Dr Zhouyang Duan for his contribution in supplying the composite film. The authors also acknowledge the financial support provided by the EPSRC grant EP/HO29923/1 and the European Research Council grant [280106-CrySys].

References

[1] M.S. San Román, M.J. Holgado, B. Salinas and V. Rives, Appl. Clay Sci. 71 (2013) 1–7.

[2] G.V. Joshi, H.A. Patel, B.D. Kevadiya, H.C. Bajaj, Appl. Clay Sci. 45 (2009) 248–253.

[3] T. Kollár, I. Pálinkó, Z. Kónya and I. Kiricsi, J. Mol. Struct. 651–653 (2003) 335–340.

[4] Y.Seki and K. Yurdakoç, Adsorption 12 (2006) 89–100.

[5] G.V. Joshi, B.D. Kevadiya, H.A. Patel, H.C. Bajaj and R.V. Jasra, Int. J. Pharm. 374 (2009) 53–57.

[6] I. Fejér, M. Kata, I. Erös, O. Berkesi and I. Dékány, Colloid. Polym. Sci. 279 (2001) 1177–1182.

[7] F.H. Lin, Y.H. Lee, C.H. Jian, J.M. Wong, M.J. Shieh and C.Y. Wang, Biomaterials 23 (2002) 1981–1987.

[8] C.D. Nunes, P.D. Vaz, A.C. Fernandes, P. Ferreira, C.C. Romão and M.J. Calhorda, Eur. J. Pharm. Biopharm. 66 (2007) 357–365.

[9] G.V. Joshi, B.D. Kevadiya and H.C. Bajaj, Microporous Mesoporous Mater. 132 (2010) 526–530.

[10] J.P. Zheng, L. Luan, H.Y. Wang, L.F. Xi and K.D. Yao, Appl. Clay Sci. 36 (2007) 297–301.

[11] M.I. Carretero, Clay minerals and their beneficial effects upon human health. A review. Appl. Clay Sci. 21 (2002) 155–163.

[12] Y. Dong and S.S. Feng, Biomaterials 26 (2005) 6068–6076.

[13] M. Datta, Appl. Clay Sci. 80–81 (2013) 85–92.

[14] Y.H. Lee, T.F. Kuo, B.Y. Chen, Y.K. Feng, Y.R. Wen, W.C. Lin and F.H. Lin, Biomed Eng-App Bas C 17 (2005) 72–78.

[15] W.F. Lee and Y.C. Chen, J. Appl. Polym. Sci. 91 (2004) 2934–2941.

[16] W.F. Lee and Y.T. Fu, J. Appl. Polym. Sci. 89 (2003) 3652–3660.

[17] S.S. Feng, L. Mei, P. Anitha, C.W. Gan and W. Zhou, Biomaterials 30 (2009) 3297–3306.

[18] Z. Duan, N.L. Thomas and W. Huang, J Membrane Sci. 445 (2013) 112–118.

[19] R. Suresh, S.N. Borkar, V.A. Sawant, V.S. Shende and S.K. Dimble, Int. J. Pharm. Sci. Drug Res. 3 (2010) 901−905.

[20] J.H. Lee, T.G. Park and H.K. Choi, Int. J. Pharm. 196 (2000) 75–83.

[21] K.I. Shimokawa, K. Saegusa, Y. Wada and F. Ishii, Colloids Surf. B, 104 (2013) 1–4.

[22] M.K. Lai and R.C.C. Tsiang, J. Microencapsul. 21 (2004) 307–316.

[23] M. Pluta, Polymer 45 (2004) 8239–8251.

[24] A. Billon, B. Bataille, G. Cassanas and M. Jacob, Int. J. Pharm. 203 (2000) 159–168.

[25] P. Kashyap, H. Dhongade, K. Singh, A. Ansari and P. Bhagel, Int. J. Med. Pharm. Sci. 1 (2011) 1–5.

[26] B. Ward and J.M. Alexander-Williams, Acute Pain 2 (1999) 139–149.

[27] H. Fessi, F. Puisieux, J.P. Devissaguet, N. Ammoury and S. Benita, Int. J. Pharm. 55 (1989) R1−R4.

[28] M. Chorny, I. Fishbein, H.D. Danenberg and G. Golomb, J. Controlled Release 83 (2002) 389–400.

[29] S. Galindo-Rodriguez, E. Allémann, H. Fessi and E. Doelker, Pharm. Res. 21 (2004) 1428–1439.

[30] R. Karnik, F. Gu, P. Basto, C. Cannizzaro, L. Dean, W. Kyei-Manu and et al., Nano Lett. 8 (2008) 2906–2912.

[31] A.J. DeMello, Nature, 442 (2006) 394–402.

[32] J. deMello and A. deMello, Lab Chip 4 (2004) 11N–15N.

[33] A.S. Utada, L.Y. Chu, A. Fernandez-Nieves, D.R. Link, C. Holtze and D.A. Weitz, MRS Bull. 32 (2007) 702–708.

[34] G.T. Vladisavljević, A. Laouini, C. Charcosset, H. Fessi, H.C.H. Bandulasena and R.G. Holdich, Colloid Surface A 458 (2014) 168–177.

[35] A. Laouini, K.P. Koutroumanis, C. Charcosset, S. Georgiadou, H. Fessi, R.G. Holdich and G.T. Vladisavljević, ACS Appl. Mater. Interfaces 5 (2013) 8939–8947.

[36] R. Othman, G.T. Vladisavljević and Z.K. Nagy, Chem. Eng. Sci. 137 (2015) 119–130.

[37] R. Othman, G.T. Vladisavljević and Z.K. Nagy, Chem. Eng. J. 280 (2015) 316–329.

[38] D.D. Joseph and H.H. Hu, in P.L. Sachdev and M. Venkatachalappa, (Eds.), Interfacial tension between miscible liquids, Recent Advances in Fluid Dynamics. CRC Press, Amsterdam, 1999, 137–156.

[39] W. Wang, S. Zhou, L. Sun and C. Huang, Carbohydr. Polym. 79 (2010) 437–444.

[40] A.K. Behera, S. Shah and B.B. Barik, Der Pharmacia Lettre 5 (2013) 43–50.

[41] D. Zheng, X. Li, H. Xu, X. Lu, Y. Hu and W. Fan, Acta Biochim. Biophys. Sinica 41 (2009) 578–87.

[42] British Standards Institution. Methods for determination of particle size distribution- Part 8: Photon correlation spectroscopy, 1997, p. BSI 11–1998.

[43] R.A. Granberg and Å.C Rasmuson, J. Chem. Eng. Data 44 (1999) 1391–1395.

[44] C. Witschi and E. Doelker, J. Control. Release 51 (1998) 327–341.

[45] T. Niwa, H. Takeuchi, T. Hino, N. Kunou and Y. Kawashima, J. Controlled Release 25 (1993) 89−98.

[46] A. Laouini, C. Charcosset, H. Fessi, R.G. Holdich and G.T. Vladisavljević, RSC Adv. 3 (2013) 4985–4994.

[47] A. Laouini, C. Charcosset, H. Fessi, R.G. Holdich and G.T. Vladisavljević, Colloids Surf., B 112 (2013) 272–278.

[48] A. Jahn, S.M. Stavis, J.S. Hong, W.N. Vreeland, D.L. DeVoe and M. Gaitan, ACS Nano 4 (2010) 2077−2087.

[49] E.E. Ekanem, S.A. Nabavi, G.T. Vladisavljević and S. Gu, ACS Appl. Mater. Interfaces 7 (2015) 23132–23143.

[50] M. Batra, S. Gotam, P. Dadarwal, R. Nainwani and M. Sharma, J. Pharm. Sci. Tech. 3 (2011) 709–716.

[51] K. Khanmohammadi, A.B. Garmarudi, N. Moazzen and K. Ghasemi, J. Struct. Chem. 51 (2010) 693–698.

[52] S. Izumikawa, S. Yoshioka, Y. Aso and Y. Takeda, J. Control. Release 15 (1991) 133–140.

[53] H.A. Patel, R.S. Somani, H.C. Bajaj, R.V. Jasra, Curr. Sci. 92 (2007) 1004−1009.

Table 1

The effect of paracetamol-to-excipient mass ratio in the organic phase and the type of excipient on the average particle size, drug encapsulation efficiency and drug loading of the prepared NPs at Q_{aq}/Q_{or} = 10 (n = 3).

PCM/excipient mass ratio in organic phase	Type of excipient			
	PLA	PLA/ 2% MMT	PLA	
	Average size of NPs, Z_{ave} (nm)		E.E. (%)	D.L. (%)
0.20	285 ± 13.4	296 ±10.4	35.2	5.9
0.45	320 ± 19.4	357 ± 11.0	32.8	10.2
0.70	398 ± 12.6	428 ± 29.4	26.6	10.9

* Note: Each analysis was repeated three times (n = 3) and the average particle sizes were determined. The error bars are standard deviations.

Table 2

The effect of Q_{aq}/Q_{or} and MMT content in the polymer matrix on the average particle size, drug encapsulation efficiency and drug loading (n = 3).

Excipient	PCM/excipient ratio = 0				PCM/excipient mass ratio = 0.2			
	PLA	PLA/ 2% MMT	PLA/ 5% MMT	PLA/ 20% MMT	PLA		PLA/ 2% MMT	
Q_{aq}/Q_{or}	Average size of blank NPs, Z_{ave} (nm)				E.E. (%)	D.L. (%)	E.E. (%)	D.L. (%)
1.5	270±34	431±6.6	434±54	666±65	27.6	4.6	29.4	4.9
3.0	276±21	383±11	441±37	629±64	27.2	4.5	31.1	5.2
4.5	237±1.8	379±5	393±36	604±88	32.5	5.4	34.3	5.7
7.0	316±7	327±4	348±11	575±62	30.7	5.1	34.7	5.8
10.0	265±24	296±10	308±14	512±10	35.2	5.9	38.5	6.4

* Note: Each analysis was repeated three times (n = 3) and the average particle sizes were determined. The error bars are standard deviations.

Table 3
Elemental composition of different samples of the prepared NPs obtained using EDS (n = 3).

Chemical element (wt%)	PLA	PLA+2 w% MMT	PLA+5w% MMT	PLA+20w% MMT	PCM-loaded PLA	PCM-loaded PLA + 2 w% MMT
C	85.90 ± 0.31	70.00 ± 0.37	21.5 ± 0.35	24.10 ± 0.22	95.00 ± 0.28	91.1 ± 0.25
O	2.59 ± 0.20	12.00 ± 0.21	37.1 ± 0.31	33.60 ± 0.21	2.34 ± 0.20	0.17 ± 0.04
Mg	0.00 ± 0.00	0.29 ± 0.08	1.83 ± 0.39	0.69 ± 0.12	0.00 ± 0.00	0.03 ± 0.01
Al	0.00 ± 0.00	1.62 ± 0.25	9.72 ± 0.25	12.10 ± 0.18	0.00 ± 0.00	0.81 ± 0.03
Si	0.00 ± 0.00	4.22 ± 0.19	16.8 ± 0.38	16.80 ± 0.16	0.00 ± 0.00	2.20 ± 0.21
K	0.00 ± 0.00	0.20 ± 0.12	4.62 ± 0.21	2.10 ± 0.30	0.00 ± 0.00	0.02 ± 0.08
Fe	0.00 ± 0.00	2.67 ± 0.43	2.61 ± 0.30	2.39 ± 0.13	0.00 ± 0.00	0.15 ± 0.04
Cu	11.50 ± 0.25	8.04 ± 0.15	5.76 ± 0.26	8.15 ± 0.12	2.69 ± 0.25	5.49 ± 0.13

* Note: Each analysis was repeated three times (n = 3) and the average values were determined. The error bars are standard deviations.

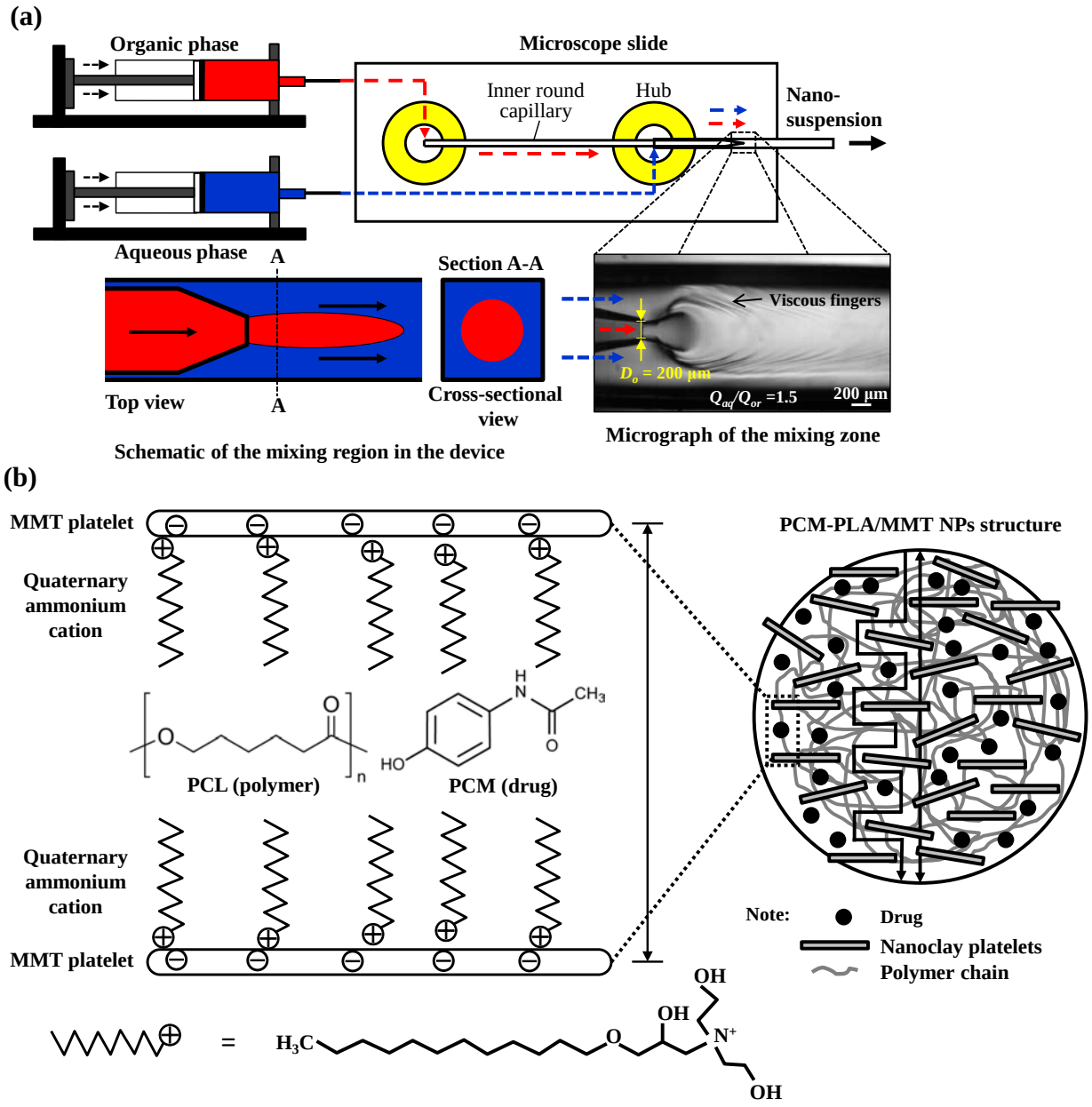

Fig. 1. Synthesis of NPs in a co-flow glass capillary device: (a) Experimental set-up consisting of two syringe pumps, plastic tubing and two coaxial capillaries glued onto a microscope slide. (b) Possible structure of encapsulated PCM-PLA/MMT NPs. Polycaprolactone (PCL) chains and paracetamol (PCM) are present between individual MMT platelets modified with a quaternary ammonium salt.

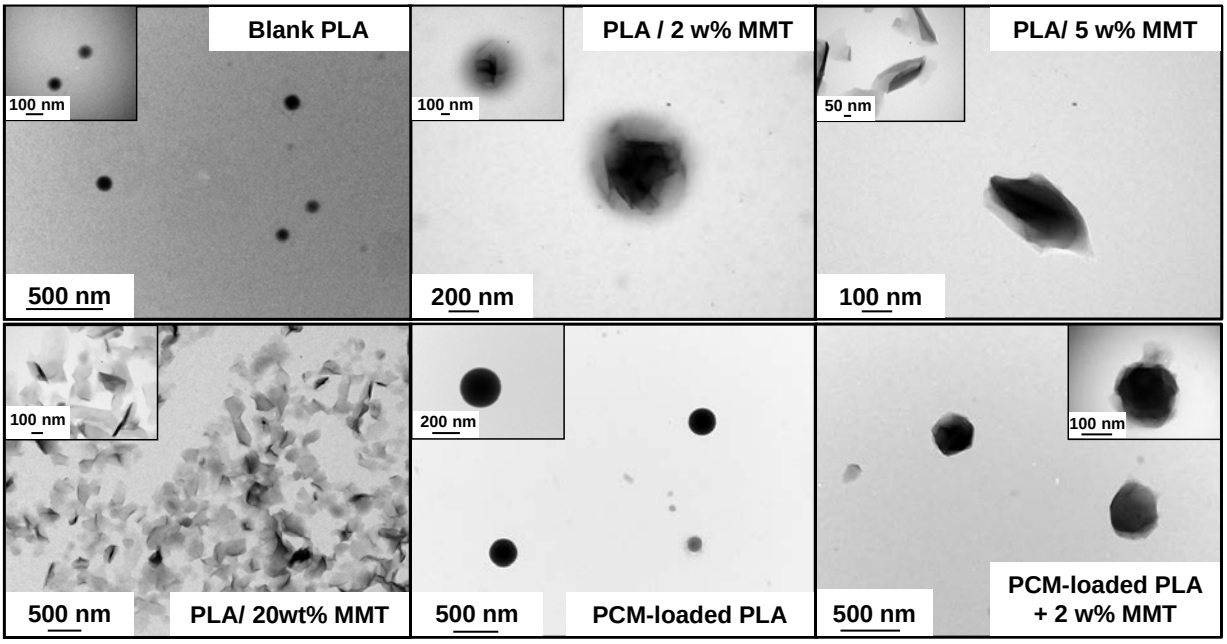

Fig. 2. TEM images of multi-functionalised NPs composed of different ratio of MMT and drug-loaded NPs prepared using the drug-to-excipient mass ratio in the organic phase of 0.2 at various magnifications.

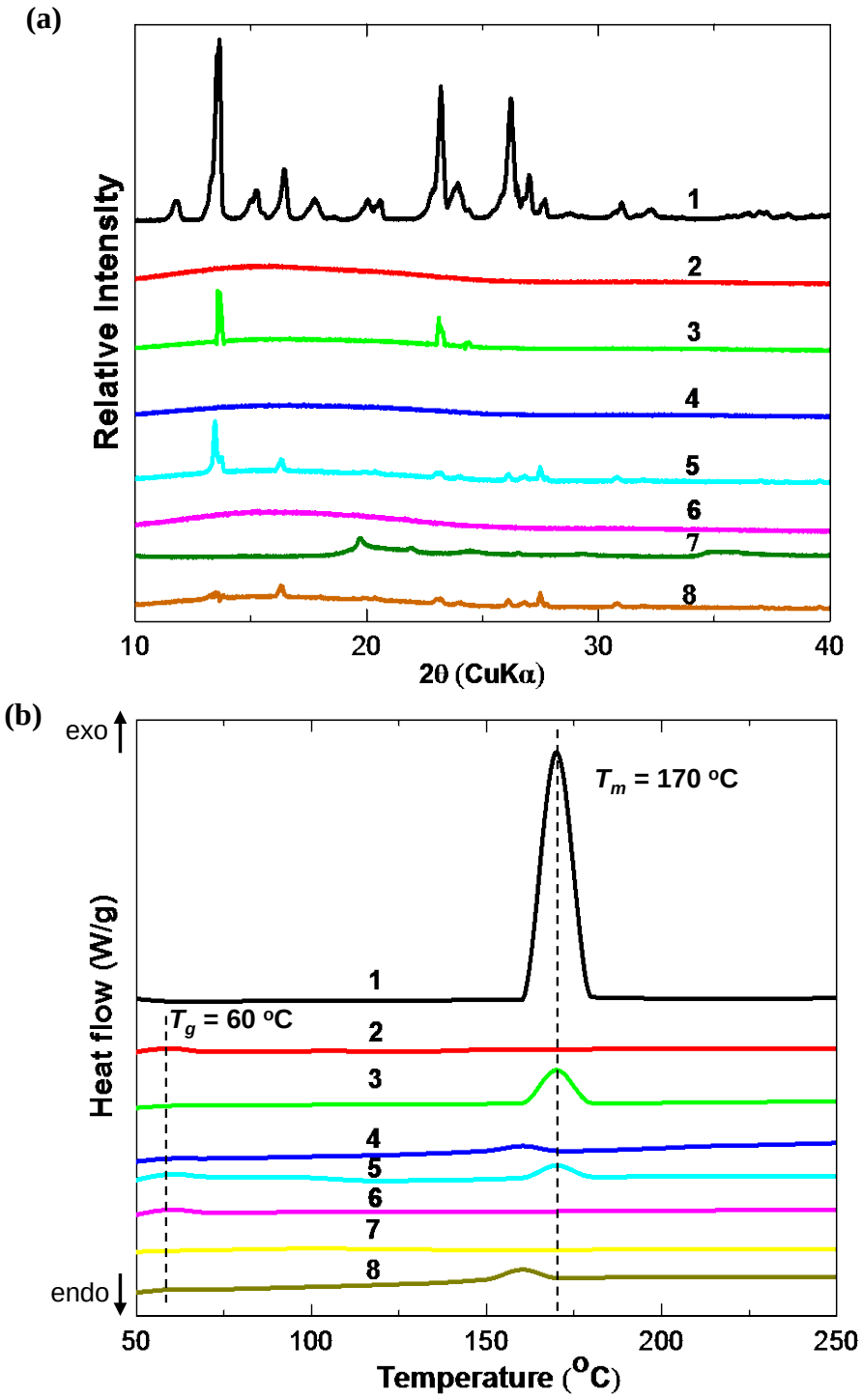

Fig. 3. (a) X-ray diffractograms and (b) DSC thermograms of; 1- pure PCM; 2- pure PLA; 3- physical mixture of PCM and PLA; 4- PCM-loaded PLA NPs; 5- physical mixture of PCM and PLA/MMT; 6- PLA/MMT composite film; 7- pure MMT and 8- PCM-loaded PLA/MMT NPs.

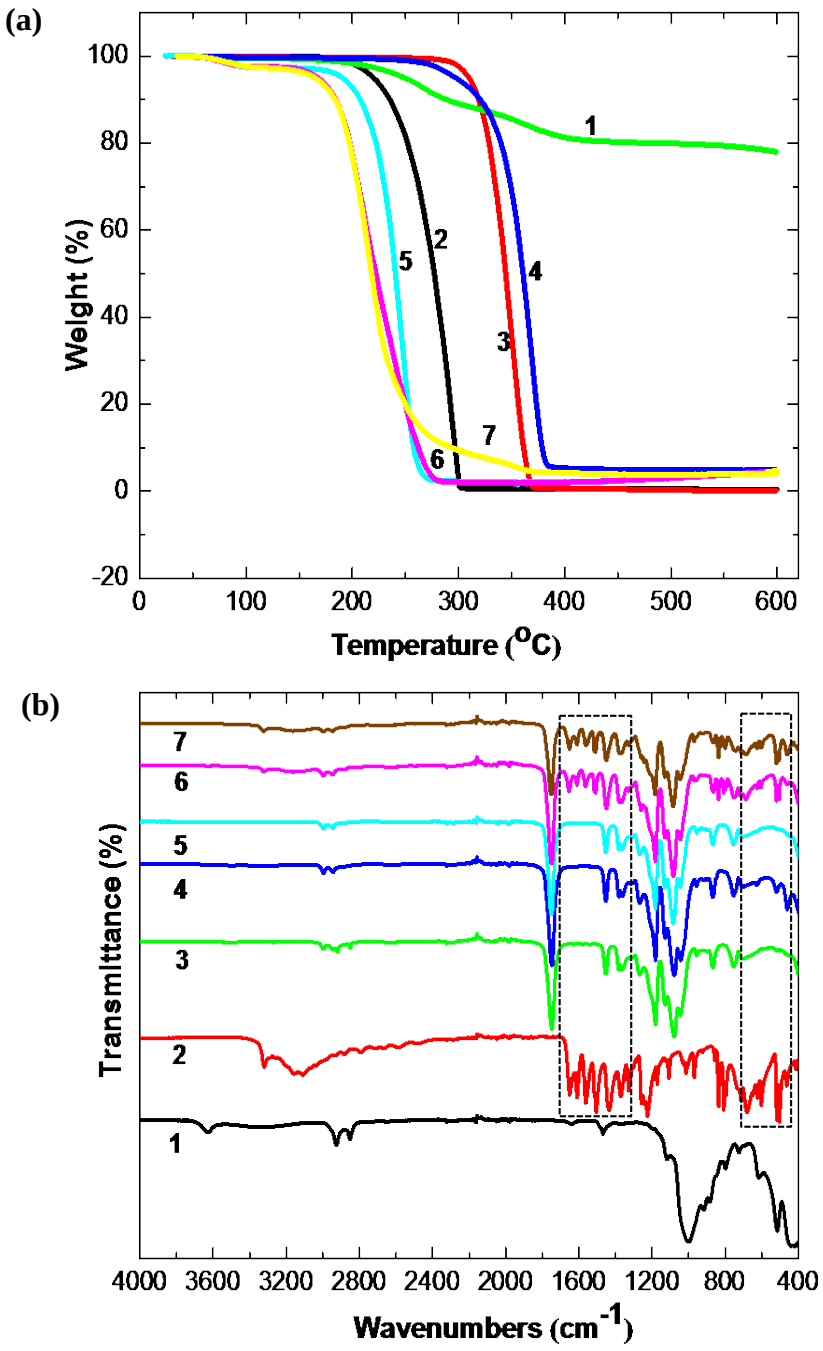

Fig. 4. (a) TGA curves and (b) FTIR spectrums of: 1- pure MMT; 2- pure PCM; 3- pure PLA; 4- PLA/MMT composite film; 5- blank PLA NPs; 6- PCM-loaded PLA NPs; 7- PCM-loaded PLA/MMT NPs.

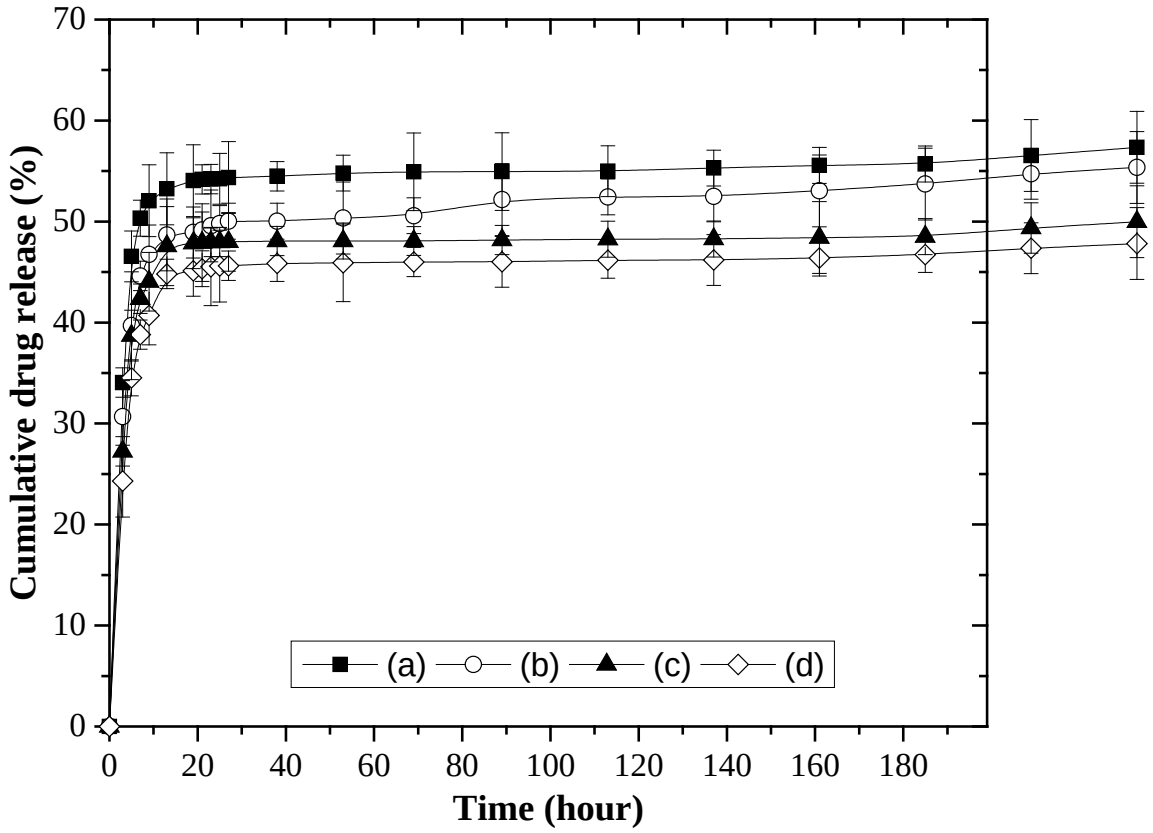

Fig. 5. In vitro release profile of paracetamol (PCM) from: (a) PLA NPs in Milli-Q water; (b) PLA NPs in phosphate-buffered saline (pH 7.4); (c) PLA/MMT NPs in Milli-Q water; (d) PLA/MMT NPs in phosphate-buffered saline (pH 7.4). The error bars represent the standard deviations of three repeated measurements (n = 3).